Dalton Transactions

PAPER

View Article Online
View Journal | View Issue

Open Access Article. Published on 22 February 2019. Downloaded on 10/24/2025 8:30:16 AM.
This article is licensed under a Creative Commons Attribution 3.0 Unported Licence.

Check for updates

Cite this: *Dalton Trans.*, 2019, **48**, 3893

Dinuclear lanthanide complexes supported by a hybrid salicylaldiminato/calix[4]arene-ligand: synthesis, structure, and magnetic and luminescence properties of $(HNEt_3)[Ln_2(HL)(L)]$ (Ln = Sm^{III}, Eu^{III}, Gd^{III}, Tb^{III})†

Steve Ullmann,[a] Peter Hahn,[a] Laura Blömer,[a] Anne Mehnert,[a] Christian Laube,[b] Bernd Abel[c,b] and Berthold Kersting *[a]

Received 21st January 2019,
Accepted 22nd February 2019

DOI: 10.1039/c9dt00292h

rsc.li/dalton

The synthesis, structures, and properties of a new calix[4]arene ligand with an appended salicylaldimine unit (H_4L = 25-[2-((2-methylphenol)imino)ethoxy]-26,27,28-trihydroxy-calix[4]arene) and four lanthanide complexes $(HNEt_3)[Ln_2(HL)(L)]$ (Ln = Sm^{III} (**4**), Eu^{III} (**5**), Gd^{III} (**6**), and Tb^{III} (**7**)) are reported. X-ray crystallographic analysis (for **4** and **6**) reveals an isostructural series of dimeric complexes with a triply-bridged $NO_3Ln(\mu\text{-}O)_2(OH\cdots O)LnO_3N$ core and two seven coordinated lanthanide ions. According to UV-vis spectrometric titrations in MeCN and ESI-MS the dimeric nature is maintained in solution. The apparent stability constants range between $\log K$ = 5.8 and 6.3. The appended salicylaldimines sensitize Eu^{III} and Tb^{III} emission (λ_{exc} 311 nm) in the solid state or immersed in a polycarbonate glass at 77 K (for **5**, **7**) and at 295 K (for **7**).

Introduction

Calix[4]arenes[1] have turned out to be versatile backbones for multidentate supporting ligands,[2,3] and a large number of donor groups have been appended at the lower and upper rim in order to control the properties of the resulting complexes.[4–17] Lanthanide complexes of such ligands have also been well investigated,[18–24] particularly for their potential in liquid–liquid extraction.[25–34] Recently, some research in this area has been directed towards the development of lanthanide-based single-molecule magnets[35] and luminescent probes and materials.[36–40] The calixarenes are typically designed to saturate the metal's coordination sphere, and several luminescent complexes have been investigated.[41–46] Despite the maturity of the field, not many lanthanide complexes of pendant calix[4]arenes were structurally characterized. Most structures are derived from calix[4]arene diamides[47] or tetraamides.[48] Only a handful of structures with triply appended calix[4]arenes have been reported,[49] and as far as we are concerned no structures exist with one-armed calix[4]arenes.[50] To fill this gap, we decided to prepare a mono-substituted calix[4]arene-Schiff base ligand H_4L and investigate its coordination chemistry towards some lanthanide ions. Hybrid ligands of this sort are known to complex first-row transition metals readily, but their lanthanide chemistry remains largely unexplored.[51–57]

This study demonstrates that H_4L supports dinuclear lanthanide complexes (for Ln = Sm, Gd, Eu, and Tb) – a property which contrasts the mononucleating behavior of the double and fourfold functionalized calix[4]arene amides. Their synthesis and characterization along with the investigation of photophysical, magnetic and structural properties are presented herein.

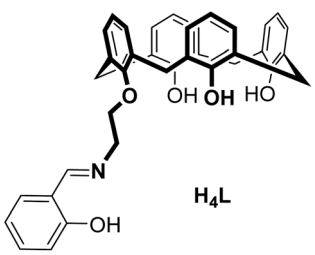

[a]Institut für Anorganische Chemie, Universität Leipzig, Johannisallee 29, 04103 Leipzig, Germany. E-mail: b.kersting@uni-leipzig.de; Fax: +49(0)341-97-36199
[b]Wilhelm-Ostwald-Institut für Physikalische und Theoretische Chemie, Universität Leipzig, Linnéstraße 2, D-04103 Leipzig, Germany
[c]Leibniz Institute for Surface Engineering (IOM), Department Functional Surfaces, D-04318 Leipzig, Germany

† Electronic supplementary information (ESI) available. CCDC 1880057–1880059. For ESI and crystallographic data in CIF or other electronic format see DOI: 10.1039/c9dt00292h

Open Access Article. Published on 22 February 2019. Downloaded on 10/24/2025 8:30:16 AM.
This article is licensed under a Creative Commons Attribution 3.0 Unported Licence.

Results and discussion

Synthesis and characterization of the ligand

The salicylaldimine-appended calix[4]arene H_4L was readily prepared according to a procedure reported by Zhang *et al.* for related bis(salicylaldimine)-*p-tert*-butylcalix[4]arenes (Scheme 1).[58] Alkylation of the parent calix[4]arene **1** with bromoacetonitrile followed by reduction of the nitrile **2** provided the amine **3**, which was condensed with salicylaldehyde in the presence of $MgSO_4$, to provide the title compound as a pale-yellow solid in 21% overall yield. The IR spectrum of H_4L reveals two sharp (3635 and 3500 cm^{-1}) and one broad OH band (3320 cm^{-1}) indicative of hydrogen bonding interactions.[59] The CN stretch appears at 1635 cm^{-1}, a typical value for salicylaldimines.[60] The calixarene adopts a *cone* conformation in CH_2Cl_2 as evidenced by NMR (two characteristic AB systems for the Ar–CH_2–Ar groups).[61–63] The free ligand displays intense absorption bands in the UV (Table 1), attributed to $\pi \rightarrow \pi^*$ transitions of aromatic rings of the calix[4]arene (254, 286 nm)[64] and the salicylaldimine (311 nm).[65,66] A weak band around 403 nm (ε = 117 M^{-1} cm^{-1}) can be assigned to the $n \rightarrow \pi^*$ transition of the imine group.

The crystal structure of the free ligand (Fig. 1) shows a *cone* conformation stabilized by three intramolecular OH···O hydrogen bonds (O1···O2, O2···O3, O3···O4). The pendant Schiff-base is almost perfectly planar forming an intramolecular

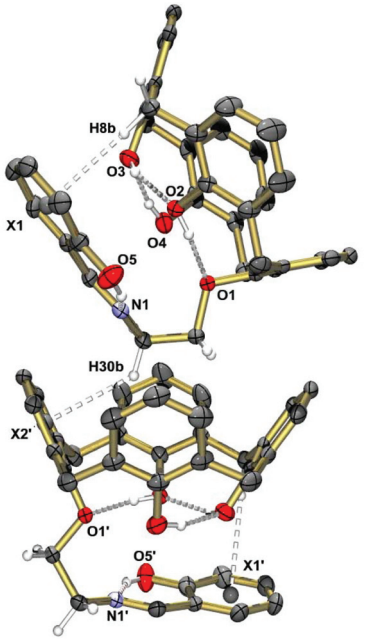

Fig. 1 Solid-state structure of compound H_4L as determined by single-crystal X-ray diffraction. Selected distances [Å]: O1···O2 2.668(3), O2···O3 2.628(3), O3···O4 2.693(3), O4···O1 2.981(3), O5···N1 2.609(3); H8b···X1 2.84, H30b···X2′ 2.90. Symmetry code used to generate equivalent atoms: $-x$, $0.5 + y$, $0.5 - z$ (′).

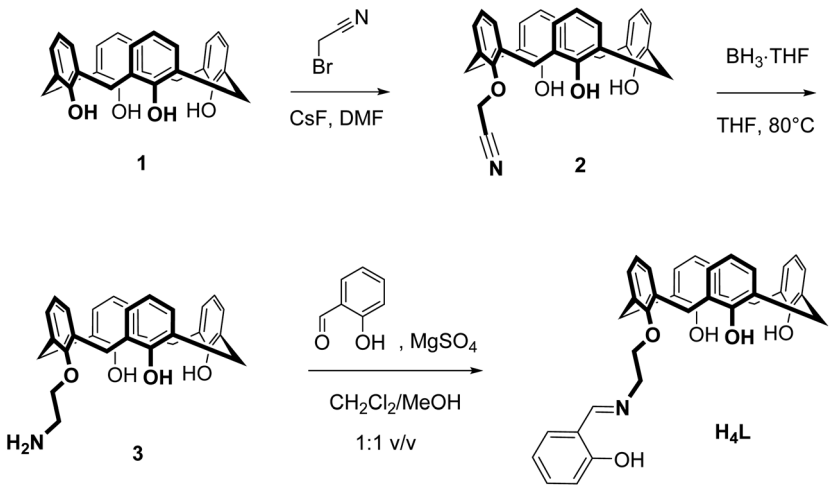

Scheme 1 Synthesis of the ligand H_4L.

Table 1 Selected analytical data for H_4L and its lanthanide complexes **4–7**[a]

Compound	ESI-MS(−)	IR/cm^{-1}	λ_{max}/nm (ε/M^{-1} cm^{-1})[b]
H_4L	570.3	1635, 1338	254 (13 397), 286 (8446), 311 (6321), 403 (117)
4 (Sm)	1439.2, 719.1	1635, 1316	299 (9874), 346 (4417)
5 (Eu)	1441.3, 720.1	1636, 1317	300 (9845), 346 (4662)
6 (Gd)	1451.3, 725.1	1636, 1325	300 (9742), 346 (4513)
7 (Tb)	1453.3, 726.1	1637, 1303	300 (9941), 344 (4367)

[a] Concentration of solutions were ~1.0×10^{-5} M, T = 298 K. [b] MeCN solution.

 This journal is © The Royal Society of Chemistry 2019

Open Access Article. Published on 22 February 2019. Downloaded on 10/24/2025 8:30:16 AM.
This article is licensed under a Creative Commons Attribution 3.0 Unported Licence.

OH···N hydrogen bond, as in other *o*-hydroxyaryl Schiff bases.[67] An intramolecular CH···π interaction manifests itself by a short H8b···X1^{centroid} distance of 2.84 Å. Self-inclusion mediated by intermolecular CH_2···π interactions of length 2.90 Å occurs. This leads to one-dimensional chains as illustrated in Fig. 1.

The new ligand and all intermediates were characterized by IR, UV-vis, ^{1}H and ^{13}C NMR spectroscopy and electrospray ionization mass spectrometry (ESI-MS). 2D NMR experiments (NOESY, HSQC, HMBC) were used to correctly assign the chemical shifts of hydrogen and carbon atoms (ESI†).

Synthesis and characterization of complexes

The reaction of H_4L with samarium(III) nitrate hexahydrate was performed with NEt_3 as a base (pK_a 18.82, MeCN)[68] to deprotonate the phenol functions. At a ~1 : 1 : 4.5 molar ratio in a mixed CH_2Cl_2/MeOH solution at room temperature a pale-yellow solution forms, from which a dinuclear compound of composition $(NHEt_3)[Sm_2(HL)(L)]$ (**4**, where L and HL represent the fourfold and threefold deprotonated versions of H_4L) could be reproducibly obtained in 82% yield (Scheme 2).

Analogous europium(III) (**5**), gadolinium(III) (**6**) and terbium(III) complexes (**7**) were also synthesized in this manner. According to ESI-MS, mononuclear complexes of composition $[LnL]^-$ are also present (Table 1), but all attempts to isolate these entities failed. The exclusive formation of the $[Sm_2(HL)(L)]^-$ dimers may be due to a lower solubility although other factors such as packing or specific intermolecular interactions cannot be ruled out. All complexes are air-stable but hygroscopic, and exhibit good solubility in methylene chloride, chloroform and THF. They are moderately soluble in toluene, and only sparingly soluble in protic solvents.

The formulation of the complexes was ascertained in all cases by elemental analysis, mass spectrometry, IR and UV-vis spectroscopy, and in case of the Sm^{III} and Gd^{III} complexes also by X-ray crystallography. The negative ESI-MS spectra of dilute (10^{-3} M) MeCN/CH_2Cl_2 solutions exhibit molecular ion peaks at m/z = 1439.2 (**4**), 1441.3 (**5**), 1451.3 (**6**), and 1453.3 (**7**), respectively, with the correct isotopic peak pattern for dimeric $[Ln_2(HL)(L)]^-$ anions (ESI). Under these conditions, signals at m/z = 719.1 (**4**), 720.1 (**5**), 725.1 (**6**) and 726.1 (**7**) for monomeric $[LnL]^-$ species are also observed. The IR spectra of all complexes reveal a band at 1635–1636 cm^{-1} for the C═N stretching frequency, a typical value for imine functions coordinated to Ln^{III} ions.[66] O–H stretching bands were absent indicative of Ln^{III} bound phenolate groups. The C–O stretching frequency observed for H_4L at 1338 cm^{-1} is shifted to lower frequencies in the complexes (1327–1316 cm^{-1}), indicative of the coordination of the phenol ether moiety as well.[69]

Crystallographic characterization

Single crystals of $(HNEt_3)[Sm_2(HL)L(MeCN)_2]$·MeCN (**4**·3MeCN) obtained from MeCN were analyzed by X-ray diffraction. The structure comprises dinuclear $[Sm_2(HL)(L)(MeCN)_2]^-$ anions (Fig. 2), $HNEt_3^+$ cations and MeCN molecules. The latter occupy voids in the structure and the calixarene cavities, as in other structures.[70] The $HNEt_3^+$ ion is located in a cleft generated by three phenyl rings of the dimer and[71] hydrogen bonds to a MeCN solvate molecule N3···N6 2.90 Å (see Fig. S1†). Significant interactions between the $HNEt_3^+$ ion and phenolate O atoms are not observed (N3···O7 4.33 Å), presumably due to the fact that the latter are buried by the organic residues of the supporting ligand.

The complex has idealized C_2 symmetry comprising two mononuclear $Sm^{III}L$ units joined by two phenolato bridges to give a four-membered Sm_2O_2 ring, a motif quite common in lanthanide calixarene structures but herein realized from phenol groups of the salicylidene moieties.[72–74] This assembly is reinforced by a hydrogen bond between O4 and O8 of the

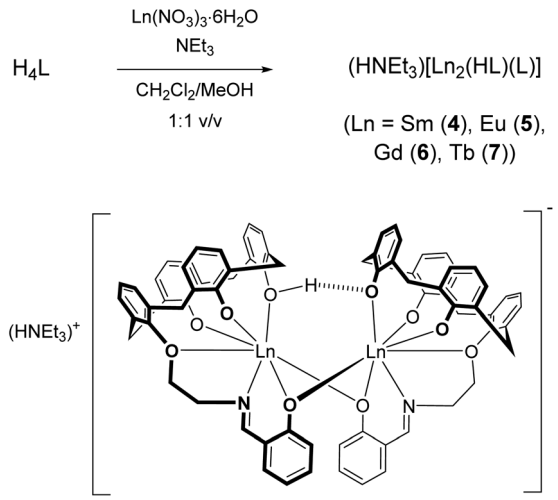

Scheme 2 Synthesis of the complexes **4**–**7**.

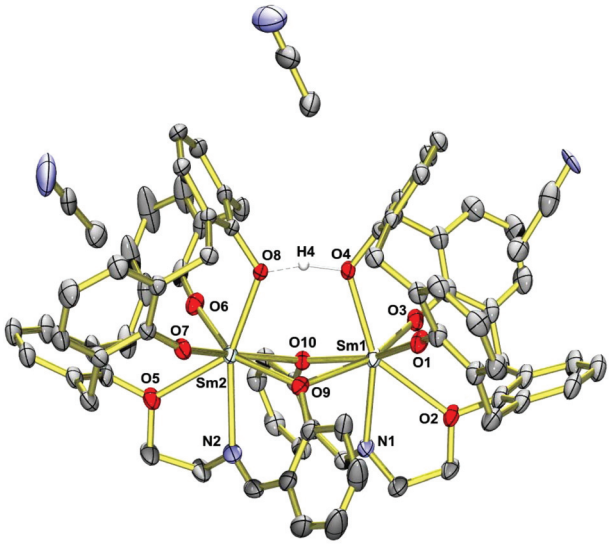

Fig. 2 Single-crystal X-ray diffraction structure of the $[Sm_2(HL)(L)(MeCN)_2]^-$ anion in crystals of $(HNEt_3)[Sm_2(HL)(L)(MeCN)_2]$·MeCN (**4**·3MeCN). The $HNEt_3^+$ ion is omitted for clarity. Thermal ellipsoids are shown at the 30% probability level.

Open Access Article. Published on 22 February 2019. Downloaded on 10/24/2025 8:30:16 AM.
This article is licensed under a Creative Commons Attribution 3.0 Unported Licence.

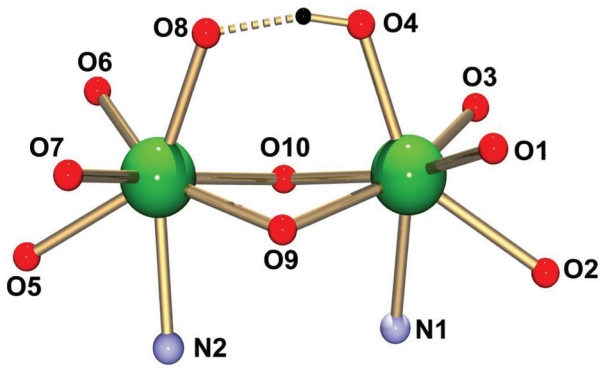

Fig. 3 Ball-and-stick representation of the immediate coordination environments of the Ln atoms in the $[Ln_2(HL)(L)(MeCN)_2]^-$ complex anions.

Table 2 Selected bond lengths [Å] and angles in $(HNEt_3)[Sm_2(HL)(L)(MeCN)_2]\cdot MeCN$ (**4**·3MeCN) and $(HNEt_3)[Gd_2(HL)(L)(MeCN)_2]\cdot MeCN$ (**6**·3MeCN)

M	**4**·3MeCN (M = Sm)	**6**·3MeCN (M = Gd)
M1–O1	2.186(2)	2.175(3)
M1–O2	2.586(3)	2.572(4)
M1–O3	2.163(3)	2.158(4)
M1–O4	2.375(2)	2.344(3)
M1–O9	2.474(2)	2.451(3)
M1–O10	2.406(2)	2.385(3)
M1–N1	2.571(3)	2.542(4)
M2–O5	2.576(3)	2.561(4)
M2–O6	2.179(3)	2.162(4)
M2–O7	2.181(3)	2.168(4)
M2–O8	2.372(2)	2.342(3)
M2–O9	2.380(2)	2.367(3)
M2–O10	2.467(2)	2.452(3)
M2–N2	2.554(3)	2.525(5)
M1···M2	3.9067(3)	3.8965(4)

calixarene bowls (O4···O8 2.40 Å, O4–H4···O8 164°).[75–77] Each samarium atom is further bonded to four calix[4]arene O atoms and to the imine N atom of the Schiff base unit, giving rise to coordination number seven (Fig. 3).

The calix[4]arene adopts a distorted cone conformation with an "elliptical" rather than a "circular" cross section very similar to that observed in $[Eu_2(HL)_2(dmf)_4]\cdot 7dmf$ (where HL represents triply deprotonated *p-t*-butyl-calix[4]arene).[74] The Sm–O bond lengths vary significantly from 2.18–2.59 Å. Four Sm–O bonds are very short (Sm1–O1,O3; Sm2–O6,O7) *ca.* 2.18 Å. The Sm–O bonds involving the bridging phenolate oxygen donors are significantly longer at 2.38–2.48 Å (Sm1–O9, O10, Sm2–O9,O10), which is not unusual for such bridges. The phenol ether O atoms (O2,O5) are weakly coordinating and form the longest Sm–O bonds (2.58 Å). They compare well with those in samarium complexes $[(pic\text{-}O)Sm\{(L\text{–}H)(EtOH)_{0.5}(CH_2Cl_2)_{0.5}\}](pic)\cdot EtOH\cdot 2H_2O$ and $[Sm(L\text{-}2H)(pic)]$, where pic = picrate anion and L is a bis- or tris-substituted calixarene.[78] The Sm–N bonds in **4** are also quite long at 2.56 Å. The presence of the hydrogen bonding interaction is supported by the relatively long Sm1–O4 and Sm2–O8 distances of 2.372 Å and 2.375 Å.

The structure of the gadolinium compound $(HNEt_3)[Gd_2(HL)L(MeCN)_2]\cdot MeCN$ (**6**·3MeCN) is isomorphous with **4**·3MeCN, having slightly shorter Gd–O and Gd–N distances (Table 2), in agreement with its smaller ionic radius.[79] The Ln···Ln distance is 3.9067(3) Å in **4** and 3.8965(4) in **6**. In essence the NO_5 donor set of H_4L cannot saturate the coordination sphere of the lanthanide ions and so dimerization occurs to share some of the O donors.[74] There are no significant intermolecular bonding interactions between the $[Ln_2(L)(HL)]^-$ complexes. The shortest intermolecular Ln···Ln distances are 10.725 Å in **4** and 10.696 Å in **6**.

Magnetic properties

The lanthanide complexes were further studied by temperature-dependent magnetic susceptibility measurements using a SQUID-Magnetometer (MPMS Quantum Design) in applied magnetic fields of 0.5 T over a temperature range 2–300 K. Plots of $\chi_M T$ *versus* T for **4–7** are shown in Fig. 4.

For the Sm_2^{III} complex **4** the $\chi_M T$ value is 0.72 cm^3 K mol^{-1} at room temperature, slightly larger than the expected value of 0.64 cm^3 K mol^{-1} for two non-interacting Sm^{III} ions.[81] On lowering the temperature, $\chi_M T$ decreases and tends to a value of *ca.* 0.01 cm^3 K mol^{-1} at 2 K. For Sm^{3+}, with a $^6H_{5/2}$ (g_J = 2/7) ground state, the multiplet spacing is on the order of k_BT and thermal population of excited $^6H_{J/2}$ states (J = 7, 9, 11, 13, 15) contributes significantly to the susceptibility. The crystal field, which partially lifts the degeneracy of the J states in zero field, may also affect the susceptibility.

We analyzed the temperature dependence of the magnetic susceptibility of the Sm^{III} complex by utilizing the analytical expression given by Kahn (eqn (S1)†).[80] This model considers only the effect of spin–orbit coupling, which is appropriate given that magnetic exchange interactions are weak as suggested by the results for the analogous Gd complex (see below). Indeed, a reasonable fit was possible (excluding the

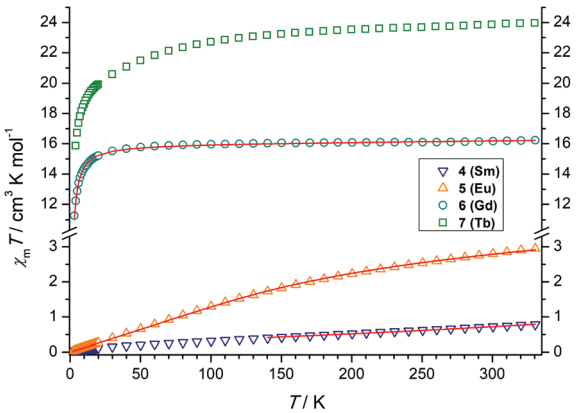

Fig. 4 Temperature dependence of the $\chi_M T$ product (at 5000 G) for the dinuclear complexes **4–7**, χ_m being the molar susceptibility per dinuclear complex defined as M/H. The solid lines correspond to the best fits.

Open Access Article. Published on 22 February 2019. Downloaded on 10/24/2025 8:30:16 AM.
This article is licensed under a Creative Commons Attribution 3.0 Unported Licence.

low temperature data). The value of the spin–orbit coupling constant was determined to be λ = 254 cm^{-1}. This value is comparable to that of the free Sm^{3+} ion (284 cm^{-1}).[81]

The $\chi_M T$ value of the Gd_2^{III} complex **6** amounts to 16.16 cm^3 K mol^{-1} at 300 K, somewhat larger than the expected value 15.77 cm^3 K mol^{-1} of two uncoupled $^8S_{7/2}$ centers. Upon cooling, $\chi_M T$ slowly decreases to 15.5 cm^3 K mol^{-1} at 23.3 K and drops to 11.2 cm^3 K mol^{-1} at 3 K, indicative of a very weak antiferromagnetic exchange interaction as in other phenolato-bridged Gd_2^{III} complexes.[82,83] For Gd^{III} ions, first-order spin–orbit coupling is absent (L = 0). Therefore, the exchange interaction can be analyzed by using the isotropic spin Hamiltonian $H = -J \cdot S_{Gd1} \cdot S_{Gd2}$ with $S_{Gd1} = S_{Gd2} = {}^7/_2$. The magnetic susceptibility for a dinuclear Gd^{III} complex is given by eqn (1), where g is the Landé factor, μ_B the Bohr magneton, N_a the Avogadro number, k_B the Boltzmann constant, and $x = J/k_B T$.[84]

$$\chi_M T = \frac{2N_a {\mu_B}^2}{k_B} \left[\frac{e^x + 5e^{3x} + 14e^{6x} + 30e^{10x} + 55e^{15x} + 91e^{21x} + 140e^{28x}}{1 + 3e^x + 5e^{3x} + 7e^{6x} + 9e^{10x} + 11e^{15x} + 13e^{21x} + 15e^{28x}} \right] \quad (1)$$

A good fit of the experimental data is possible applying J = −0.065 cm^{-1} and g = 2.01. Such a weak antiferromagnetic coupling constant is a typical value for phenolato-bridged Gd^{III} systems.[82,84–87]

The $\chi_M T$ value of the Eu_2^{III} complex **5** is 2.80 cm^3 K mol^{-1} at 300 K, a value which is close to that expected for two non-interacting Eu^{III} ions (2.65 cm^3 K mol^{-1}), with non-negligible population of excited $^7F_1$–$^7F_6$ levels. The deviation from the Hund-Landé expectation value (0μ_B) is also attributable to contributions from the second order Zeeman effect in the ground $^7F_0$ multiplet.[88] Upon cooling, the $\chi_M T$ values decrease steadily, reaching 0.03 cm^3 K mol^{-1} at 2 K, as in other dinuclear Eu^{III} complexes.[89] The magnetic susceptibility of the Eu_2^{III} complex can be fitted to the formula derived by Kahn (eqn (S2)†) by considering only λ (multiplet spacing) as a parameter as also done for the Sm^{III} complex. Again, the magnetic interaction between the Eu^{III} ions are assumed negligible.

Indeed, an excellent fit was possible over the whole temperature range to give λ = 324 cm^{-1}. The multiplet spacing is within the range of k_BT, and significant population of the first excited state at 300 K explains the deviation from the Curie law. The λ parameter for **6** agrees with other dinuclear Eu^{III} complexes. In $[Eu_2(L')_2]$, for example, where L′ is derived from a calixarene ligand with two hydroxyquinolinolato arms, and the Eu^{III} ions in an N_4O_4 environment λ = 325 cm^{-1}.[90]

The $\chi_M T$ value of the dinuclear Tb^{III} complex at 300 K with 23.87 cm^3 K mol^{-1} is slightly higher than the expected value of 23.60 cm^3 K mol^{-1} for a $^7F_6$ ground state. Upon cooling the $\chi_M T$ values decrease first slowly to 22.71 cm^3 K mol^{-1} at 100 K and then more rapidly to 15.87 cm^3 K mol^{-1} at 4 K. Tb^{III} complexes are known to exhibit significant magnetic anisotropy, and fitting of susceptibility data is therefore difficult.[84] The field dependence of the magnetization for complex **7** was determined in order to see whether magnetic anisotropy is present in this complex. Indeed, at 2 K the magnetization values increase rapidly at low fields and then linearly but without a clear saturation, reflecting the presence of a significant magnetic anisotropy (Fig. 5). Moreover, a M *vs.* H/T plot (Fig. 6) illustrates that the curves are not really superimposed on each other as expected for an isotropic system with a well-defined ground state. Nevertheless, hysteresis effects were not observed in M *vs.* H data at 2 K. Alternative current (ac) measurements were also undertaken to determine potential SMM behavior. However, neither maxima nor imaginary components of the ac susceptibility were observed in the χ''_M *vs.* T plots, ruling out an SMM behavior for **7**. This may be attributed to the low local symmetry of the Tb^{III} ions.[91]

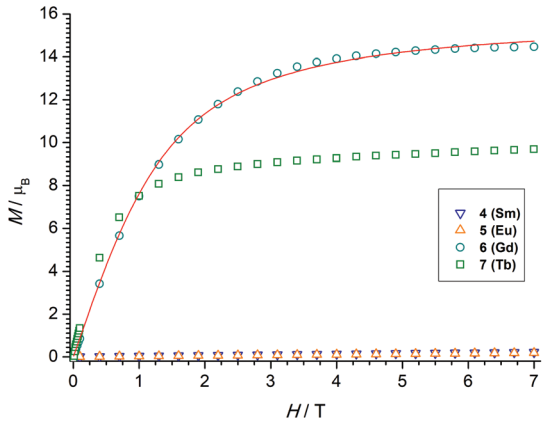

Fig. 5 Field dependence of the magnetization for powdered samples of **4–7** at 2 K.

Spectrophotometric titrations

To study the complexation reactions of H_4L with Sm^{III}, Eu^{III}, Gd^{III}, and Tb^{III} in solution UV-vis spectrophotometric batch titrations were carried out. The experiments were performed at

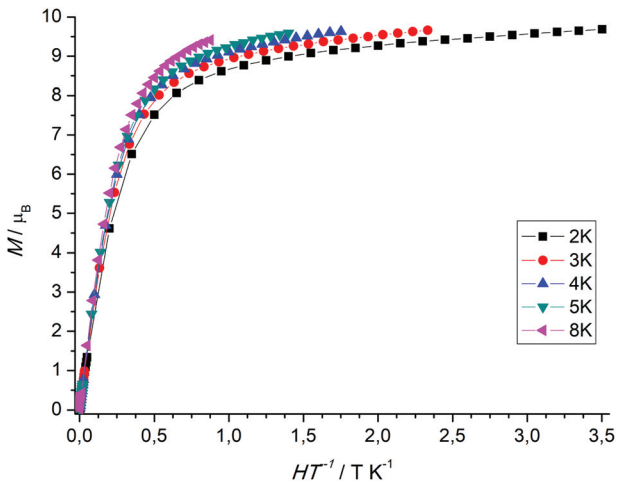

Fig. 6 Plot of M *versus* H/T for the Tb^{III} complex **7** at various temperatures.

Open Access Article. Published on 22 February 2019. Downloaded on 10/24/2025 8:30:16 AM.
This article is licensed under a Creative Commons Attribution 3.0 Unported Licence.

room temperature in acetonitrile at constant ionic strength (10^{-2} M nBu$_4$NPF$_6$) and pH value (5×10^{-4} M NEt$_3$ buffer). Data were recorded in the 200–600 nm range. The titration of H$_4$L with Sm(NO$_3$)$_3$·6H$_2$O is representative for all complexes (Fig. 7). For the other compounds, see ESI Fig. S29–S35.† Upon addition of aliquots of Sm(NO$_3$)$_3$·6H$_2$O (0–5 equiv.) clear changes occur in the UV-vis ligand spectra. The bands at 254, 286, and 311 nm for H$_4$L vanish with increasing Sm^{III} concentration, while new bands (for [Sm$_2$(HL)(L)]$^-$) develop with maxima at 300 and 345 nm. The final spectra match the recorded spectra of the isolated metal complexes. An isosbestic point at 325 nm indicates that Sm^{III} binding occurs to a single equilibrium.

To determine the stoichiometry of the resulting species the mole ratio method was applied.[92] The inset of Fig. 7 shows a plot of absorbance values at 345 nm *versus* molar ratio [Sm^{III}]/[H$_4$L]. The values increase steadily up to a molar ratio of about unity and then remains constant. No further changes were observed for up to five-fold excess of lanthanide salt, signifying the formation of a complex species with 1 : 1 ligand/metal stoichiometry. The other lanthanide ions behave in a very similar fashion. Irrespective of the type of the lanthanide ion, only 1 : 1 compounds were systematically detected. Nonlinear least-squares refinements of the titration data converged for a speciation model involving the ligand and its 1 : 1 complexes with apparent stability constants of 6.08(4) (Sm^{III}), 6.21(7) (Eu^{III}), 5.81(4) (Gd^{III}), and 6.34(6) (Tb^{III}). The stability constants show a strong affinity of L^{4-} towards lanthanides and decrease with decreasing ionic radii with the strongest interaction observed with Tb^{III} and the weakest interaction observed for Sm^{III}. There are only very few studies reporting thermodynamic data for f-element calixarene complexes in non-aqueous solvents.[93–96] Danil de Namor and Jafour have studied the complexation of trivalent cations by *p-tert*-butylcalix[4]arene tetraethanoate, *p-tert*-butylcalix[4]arene tetramethyl ketone, and *p-tert*-butylcalix[4]arene tetraacetamide in acetonitrile.[97] Borisova and co-workers have determined stability constants for lanthanide complexes supported by 2,2′-bipyridyl-6,6′-dicarboxylic acid diamide and 2,6-pyridinedicarboxylic acid diamide ligands in the same solvent. The binding constants of these complexes were found to lie in a similar range (log $K \sim 4$–6).[98]

Spectroscopic and photophysical properties

The new compounds were further characterized by UV-vis absorption and emission spectroscopy. The electronic absorption spectra were measured in acetonitrile (complexes) at room temperature. Table 1 lists the data. All complexes show three intense absorption bands around 220 nm, 300 nm, and 350 nm, respectively. The first two high-energy bands are associated with $^1(\pi\text{–}\pi)^*$ transitions centered on the phenol ether and phenolate groups of the calix[4]arene backbone. The transition at 350 nm can be attributed to the phenyl ring of the salicylaldimine unit. Deprotonation and coordination of the lanthanides red-shifts these features by 15 and 40 nm relative to those of the free ligand. The change of the lanthanide ion appears to have little if any impact on the spectrophotometric properties. Hence, upon going from the Sm to the Tb complex a slight blue-shift of the lowest energy band of *ca.* 2 nm can be detected.

The luminescence properties of the Eu and Tb complexes were investigated in view of literature reports that calix[4]arenes can act as an antenna for the sensitization of lanthanide luminescence.[37,41] The free ligand shows a single emission band with a maximum at 455 nm when excited at 285 nm. The two complexes are not emissive in solution (CH$_3$CN, CH$_2$Cl$_2$). However, when embedded in a polymer Eu complex **5** displays four relatively broad and intense transitions (Fig. 8), attributed to $^5D_0 \rightarrow {}^7F_J$ transitions (J = 1–2) when excited at 311 nm at 77 K.[99] Both, the $^5D_0 \rightarrow {}^7F_1$ (580 nm, 595 nm,) and the $^5D_0 \rightarrow {}^7F_2$ transitions (620, 630 nm) appear as doublets. In view of the low local symmetry of the

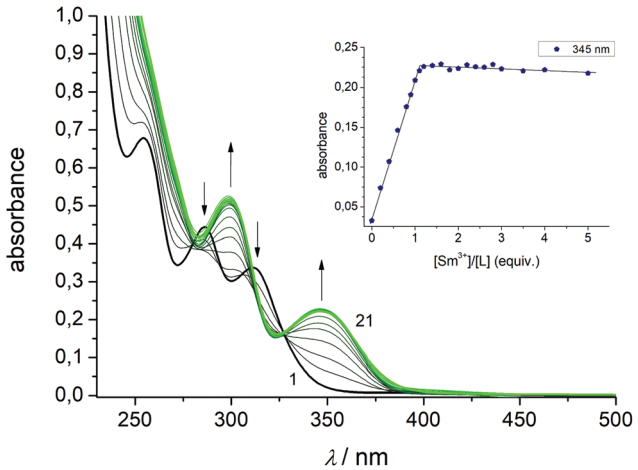

Fig. 7 Spectrophotometric titration of H$_4$L with Sm(NO$_3$)$_3$·6H$_2$O in CH$_3$CN (10^{-5} M concentration) at constant ionic strength (10^{-2} M N^{n}Bu$_4$PF$_6$, T = 298 K) in the presence of 5×10^{-4} M NEt$_3$. The green curve refers to a final molar ratio of M/H$_4$L = 5.0. The inset shows the evolution of absorbance values at 345 nm *versus* the [Sm^{III}]/[H$_4$L] molar ratio.

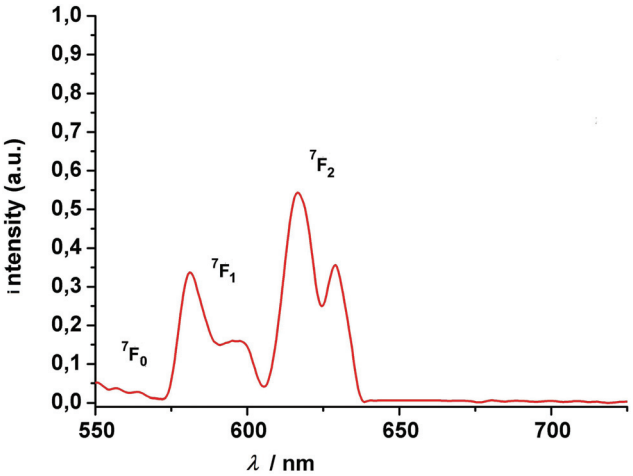

Fig. 8 Luminescence spectrum of (HNEt$_3$)[Eu$_2$(HL)(L)] (**5**) at 77 K (polycarbonate thin films doped with 4 wt% Eu). The excitation wavelength is 311 nm. The transitions above 575 nm start from the $^5D_0$ state.

 This journal is © The Royal Society of Chemistry 2019

Open Access Article. Published on 22 February 2019. Downloaded on 10/24/2025 8:30:16 AM.
This article is licensed under a Creative Commons Attribution 3.0 Unported Licence.

coordination polyhedron (C_1 in this case), this may be related to crystal-field splitting of the $^7F_1$ and $^7F_2$ levels. Splitting of these levels is not unusual for Eu(III) complexes with such a low site symmetry.[100] The $^5D_0 \rightarrow {}^7F_0$ transition (expected in the 570–585 nm range), is a strictly forbidden transition in site symmetries other than C_{nv}, C_n or C_s.[100] It is also not observed for the present compound.

The intensity of the hypersensitive $^5D_0 \rightarrow {}^7F_2$ transition (or the ratio R of the intensities $I(^5D_0 \rightarrow {}^7F_2)/I(^5D_0 \rightarrow {}^7F_1)$ is also often used as a measure for the asymmetry of the Eu^{3+} site, since the $^5D_0 \rightarrow {}^7F_2$ signal is strictly forbidden for a Eu^{3+} at a site with inversion symmetry. In our case, there is no inversion symmetry about the Eu^{3+} ion. The $^5D_0 \rightarrow {}^7F_2$ is observed and is 1.6 times more intense than the $^5D_0 \rightarrow {}^7F_1$ transition, in good agreement with the theoretical predictions.[101–103]

The Tb complex gives rise to four transitions at 490, 545, 584 and 619 nm, assigned to the $^5D_4 \rightarrow {}_7F_J$ (J = 6, 5, 4, 3) transitions, again split by crystal-field effects. Of these, the "green" $^5D_4 \rightarrow {}^7F_5$ transition at 545 nm has the highest intensity. Note that the intensity decreases with increasing temperature, which might be traced to quenching *via* enhanced vibrational relaxation (energy transfer to the O–H···O vibration modes).[104,105]

The excited state luminescence decay of the immobilized Tb complex is biexponential, although the first exponential term is dominating (99% of the initializing luminescence intensity, I_0) with a lifetime of about τ_1 = 81 ± 2.5 μs. A small contribution of a second term with a time constant of τ_2 = 305 ± 3 μs was determined. The origin of the second term may be a different conformation of the complex due to the imbedding into the polymer matrix, as often observed for imbedded dyes.[106] This will be further investigated in a subsequent work. The features of the lifetimes are comparable to values reported for other luminescent Tb calixarene complexes (Fig. 9 and 10).[37,107]

The luminescence properties of the Gd compound **6** were examined in order to determine the triplet state energy of the Schiff base ligand. The emission spectrum of compound **6** embedded in polycarbonate at 77 K is strong (Fig. S38†), with the shortest wavelength 0–0 transition of the ligand peaking at *ca.* 457 nm (21 882 cm^{-1}). This triplet-state energy compares well with those of other Schiff base ligands[66] and lies well above the resonance energy levels of the Eu(III) and Tb(III) ions. These results suggest that a ligand triplet state is indeed involved in the energy transfer mechanism to the resonance state of the Ln(III) ions, from which emission occurs.

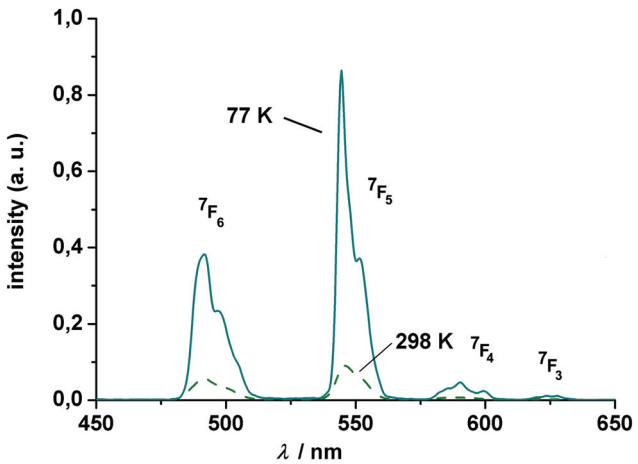

Fig. 9 Luminescence spectrum of $(HNEt_3)[Tb_2(HL)(L)]$ (**7**) at 77 and 298 K (polycarbonate thin film doped with 4 wt% Tb). The excitation wavelength is 311 nm. All transitions start from the $^5D_4$ state.

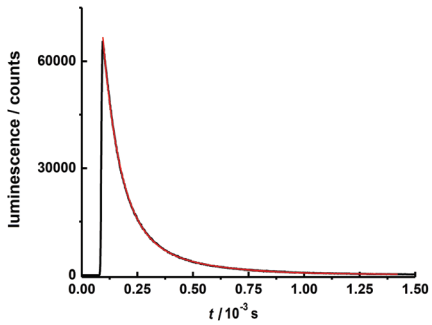

Fig. 10 Luminescence decay curve for 4 wt% $(HNEt_3)[Tb_2(HL)(L)]$ in polycarbonate matrix at 298 K after excitation at λ_{ex} = 310 nm (pulse width = 12.6 μs) detected at 545 nm within the time range of 1.5 ms.

Conclusions

A new monofunctionalized calix[4]arene-Schiff base ligand has been synthesized and its coordination chemistry towards selected lanthanide ions (Sm, Eu, Gd, Tb) investigated in solution and solid state. The chemistry of this ligand system is distinct from that of the well-studied bis- and tetrakis-lower rim functionalized calix[4]arenes, which tend to support only monomeric structures. Dimerization occurs *via* the salicylidene's phenolate groups, not *via* bridging O atoms from the calix[4]arene, as seen for some heteroleptic complexes involving the parent calix[4]arenes to give coordination number 7 with an highly irregular coordination geometry. The assembly is further stabilized by an intramolecular OH···O–hydrogen bond established in second sphere of the calixarene bowls. The dimeric units are also present in MeCN solution as suggested by ESI MS. There are little – if any – magnetic exchange interactions in the dimers, and the absence of SMM behavior may be associated with the low local symmetry of the lanthanide ions. The present study enlarges the database, may contribute to current knowledge of structure–property relationship in Ln calixarene containing SMMs, luminescent materials, and chemosensors.

Experimental section

Materials and methods

The calix[4]arene **1** was prepared as described in the literature.[108] All reagents and solvents were commercial grade and used without further purification. Melting points were deter-

Open Access Article. Published on 22 February 2019. Downloaded on 10/24/2025 8:30:16 AM. This article is licensed under a Creative Commons Attribution 3.0 Unported Licence.

mined with an Electrothermal IA9000 series instrument using open glass capillaries and are uncorrected. Elemental analyses were carried out on a VARIO EL elemental analyzer (Elementar Analysensysteme GmbH, Hanau). NMR spectra were recorded on a Bruker FT 300 spectrometer or AVANCE DRX 400 spectrometer at 298 K. Chemical shifts refer to solvent signals. Mass spectra were obtained using the negative ion electrospray ionization modus (ESI) on a Bruker Daltronics ESQUIRE 3000 Plus ITMS or Impact II UHR Qq-TOF instrument. Infrared spectra (4000–400 cm^{-1}) were recorded at 1 cm^{-1} resolution on a Bruker TENSOR 27 (equipped with a MIRacle ZnSe ATR accessory from PIKE Technologies) FT-IR spectrometer. Solution absorption spectra were collected on a Jasco V-670 UV–vis–NIR device. Steady state fluorescence absorption and emission spectra were recorded on a PerkinElmer LS 50B luminescence spectrometer using 1 cm quartz cells (Hellma). The magnetic susceptibility measurements were performed with the use of a MPMS 7XL SQUID magnetometer (Quantum Design) working between 1.8 and 330 K for applied dc fields ranging from −7 to 7 T. Measurements were performed on polycrystalline samples over the temperature range 2–330 K at applied magnetic field of 0.1, 0.5, 1.0 T. The observed susceptibility data were corrected for the underlying diamagnetism.

Synthesis and analysis of compounds

25-(2-Cyanomethoxy)-26,27,28-trihydroxy-calix[4]arene (2). Cesium fluoride (2.15 g, 14.13 mmol, 1.2 eq.) and tetrahydroxycalix[4]arene (5.00 g, 11.78 mmol) were dissolved in warm (40 °C) DMF (100 ml). Bromoacetonitrile (8.21 mL, 117.8 mmol, 10 eq.) was added and stirring continued for 2 d at 40 °C. The resulting pale-yellow suspension was acidified with 250 mL aqueous HCl (5 M) and extracted with CH_2Cl_2 (3 × 100 mL). The organic fractions were combined, dried with $MgSO_4$, and filtered. Evaporation provided an oily residue which was purified by column chromatography (CH_2Cl_2, R_f = 0.41). Colorless solid, yield: 1.59 g (29% based on **1**). M.p. 247 °C. Elemental analysis for $C_{30}H_{25}NO_4{\cdot}H_2O$ (463.53 + 18.02) calcd: C 74.83, H 5.65, N 2.91%; found C 75.10, H 5.45, N 2.78%. *m/z* (ESI−, MeCN): $C_{30}H_{25}NO_4$ (463.18) $[M - H^+]^-$ calcd: 462.17; found 462.2. ^{1}H-NMR (300 MHz, CH_2Cl_2-d_2, for atom labels see inset, Fig. S2†): δ = 3.50 (d, $^2J_{(H,H)}$ = 13.9 Hz, 2H, ArCH_{eq}HAr, $C^{8/14}$), 3.60 (d, $^2J_{(H,H)}$ = 13.4 Hz, 2H, ArC*H*eqHAr, $C^{2/20}$), 4.23 (d, $^2J_{(H,H)}$ = 13.9 Hz, 2H, ArCH*H*axAr, $C^{8/14}$), 4.35 (d, $^2J_{(H,H)}$ = 13.4 Hz, 2H, ArCH*H*axAr, $C^{2/20}$), 5.04 (s, 2H, –OCH_2, C^{29}), 6.71 (t, $^3J_{(H,H)}$ = 7.5 Hz, 1H, *p*-Ar*H*, C^{11}), 6.72 (t, $^3J_{(H,H)}$ = 7.5 Hz, 2H, *p*-Ar*H*, $C^{5/17}$), 6.93–7.04 (m, 3H, *p*-Ar*H*, *m*-Ar*H*, C^{23}, $C^{10/12}$), 7.04–7.17 (m, 6H, *m*-Ar*H*, $C^{6/16}$, $C^{22/24}$, $C^{4/18}$), 8.43 (s, 2H, Ar–O*H*, $C^{26/28}$), 9.13 (s, 1H, Ar–O*H*, C^{27}). ^{13}C{^{1}H} NMR (100 MHz, CH_2Cl_2-d_2, for atom labels see Fig. S2†): δ = 32.0 (Ar*C*H_2Ar, $C^{2/20}$), 32.1 (Ar*C*H_2Ar, $C^{8/14}$), 61.2 (O*C*H_2, C^{29}), 115.3 (*C*≡N, C^{30}), 121.5 (*p*-*C*Ar c[4]a, $C^{5/17}$), 122.6 (*p*-*C*Ar c[4]a, C^{11}), 127.8 (*p*-*C*Ar c[4]a, C^{23}), 128.1 (*o*-*C*Ar c[4]a, $C^{7/15}$), 128.6 (*o*-*C*Ar c[4]a, $C^{3/19}$), 129.05 (*o*-*C*Ar c[4]a, $C^{9/13}$), 129.1 (*m*-*C*Ar c[4]a, $C^{4/18}$), 129.4 (*m*-*C*Ar c[4]a, $C^{6/16}$), 129.6 (*m*-*C*Ar c[4]a, $C^{10/12}$), 130.5 (*m*-*C*Ar c[4]a, $C^{22/24}$), 134.1 (*o*-*C*Ar c[4]a, $C^{1/21}$), 149.3 (*ipso* *C*Ar–OH c[4]a, C^{27}), 150.9 (*ipso* *C*Ar–O–CH_2 c[4]a, C^{25}), 151.5 (*ipso* *C*Ar–OH c[4]a, $C^{26/28}$). ATR-IR (ZnSe): ν/cm^{-1} = 3290 (s, br, ν O–H), 3271 (s, br, ν O–H), 3040 (w), 2931 (w), 2866 (w), 1593 (w, ν C=C), 1467 (s, ν C=C), 1454 (s, ν C=C), 1430 (m), 1377 (m), 1349 (m), 1297 (w), 1272 (m), 1260 (m), 1243 (m), 1226 (m), 1210 (m), 1180 (m), 1156 (w), 1146 (w), 1085 (w), 1034 (m), 1029 (w), 976 (w), 959 (w), 949 (w), 908 (w), 895 (w), 841 (w), 806 (w), 796 (w), 778 (w), 753 (s), 742 (m), 705 (w), 692 (w), 686 (w).

25-(2-Aminoethoxy)-26,27,28-trihydroxy-calix[4]arene (3). The nitrile **2** (1.64 g, 3.54 mmol) was dissolved in dry THF (100 mL). The solution was cooled to 0 °C and a BH_3·THF solution (1 M, 37.3 mL, 37.3 mmol, 10.54 eq.) was added dropwise. The reaction mixture was refluxed for 12 h, cooled to r.t., and hydrolyzed with aqueous HCl (1 M, 100 mL). After stirring for 1 h, the solvent was evaporated under reduced pressure. The resulting white solid was taken up in CH_2Cl_2 (100 mL), water (20 mL) was added, and the pH adjusted to 10 by addition of aqueous NaOH solution (2 M). The organic phase was separated and the aqueous phase extracted with CH_2Cl_2 (3 × 50 mL). The organic fractions were combined and evaporated to dryness. Colorless solid, yield: 1.51 g (91% based on **2**). M. p. 239 °C. Elemental analysis for $C_{30}H_{29}NO_4{\cdot}1/2H_2O$ (467.57 + 9.01) calcd: C 75.61, H 6.35, N 2.94%; found C 75.37, H 6.38, N 2.66%. *m/z* (ESI+, MeCN/CH_2Cl_2): $C_{30}H_{29}NO_4$ (467.210) $[M + H^+]^+$ calcd: 468.217; found 468.3. ^{1}H-NMR (300 MHz, DMSO-d_6, for atom labels see Fig. S6†): δ = 3.17 (d, $^2J_{(H,H)}$ = 12.4 Hz, 2H, ArCH_{eq}HAr, $C^{8/14}$), 3.23 (d, $^2J_{(H,H)}$ = 12.0 Hz, 2H, ArCH_{eq}HAr, $C^{2/20}$), 3.47 (t, $^3J_{(H,H)}$ = 4.9 Hz, 2H, NCH_2, C^{30}), 4.07 (t, $^3J_{(H,H)}$ = 4.9 Hz, 2H, OCH_2, C^{29}), 4.10 (d, $^2J_{(H,H)}$ = 12.4 Hz, 2H, ArCHH_{ax}Ar, $C^{8/14}$), 4.31 (d, $^2J_{(H,H)}$ = 12.0 Hz, 2H, ArCHH_{ax}Ar, $C^{2/20}$), 6.15 (t, $^3J_{(H,H)}$ = 7.3 Hz, 1H, *p*-Ar*H*, C^{11}), 6.40 (t, $^3J_{(H,H)}$ = 7.4 Hz, 2H, *p*-Ar*H*, $C^{5/17}$), 6.69 (t, $^3J_{(H,H)}$ = 7.5 Hz, 1H, *p*-Ar*H*, C^{23}), 6.80 (d, $^3J_{(H,H)}$ = 7.3 Hz, 2H, *m*-Ar*H*, $C^{10/12}$), 6.85 (dd, $^3J_{(H,H)}$ = 7.5 Hz, $^4J_{(H,H)}$ = 1.7 Hz, 2H, *m*-Ar*H*, $C^{6/16}$), 6.98–7.05 (m, 4 H, *m*-Ar*H*, $C^{22/24}$, $C^{4/18}$), 10.79 (br s, 5H, –NH_2, Ar–O*H*). ^{13}C{^{1}H}-NMR (75 MHz, DMSO-d_6, for atom labels see Fig. S6†): δ = 31.1 (Ar*C*H_2Ar, $C^{2/20}$), 33.8 (Ar*C*H_2Ar, $C^{8/14}$), 40.3 (*C*H_2N, C^{30}), 69.1 (O*C*H_2, C^{29}), 114.2 (*p*-*C*Ar c[4]a, C^{11}), 117.7 (*p*-*C*Ar c[4]a, $C^{5/17}$), 123.9 (*p*-*C*Ar c[4]a, C^{23}), 127.5 (*m*-*C*Ar c[4]a, $C^{4/18}$), 127.6 (*m*-*C*Ar c[4]a, $C^{6/16}$, $C^{10/12}$), 128.1 (*m*-*C*Ar c[4]a, $C^{22/24}$), 129.4 (*o*-*C*Ar c[4]a, $C^{9/13}$), 130.4 (*o*-*C*Ar c[4]a, $C^{3/19}$), 130.5 (*o*-*C*Ar c[4]a, $C^{7/15}$), 135.0 (*o*-*C*Ar c[4]a, $C^{1/21}$), 152.5 (*ipso* *C*ArOCH_2 c[4]a, C^{25}), 154.8 (*ipso* *C*Ar–OH c[4]a, $C^{26/28}$), 159.3 (*ipso* *C*Ar–OH c[4]a, C^{27}). ATR-IR (ZnSe): ν/cm^{-1} = 3351 (w, ν O–H), 3342 (w, ν O–H), 3296 (w, ν N–H), 3291 (w, ν N–H), 2958 (w), 2924 (w), 2868 (w), 2859 (w), 2850 (w), 1590 (m, ν C=C), 1461 (s, ν C=C), 1445 (s, ν C=C), 1399 (m), 1364 (w), 1251 (m), 1212 (m), 1181 (w), 1149 (w), 1090 (m), 1079 (m), 1008 (w), 971 (w), 913 (w), 885 (w), 840 (w), 828 (w), 802 (w), 755 (s), 700 (w).

25-[2-((2-Methylphenol)imino)ethoxy]-26,27,28-trihydroxy-calix[4]arene (H_4L). To a solution of **3** (0.50 g, 1.07 mmol) and salicylaldehyde (144 mg, 1.18 mmol) in CH_2Cl_2/MeOH (150 mL, 1 : 1, v/v) was added $MgSO_4$ (100 mg). The resulting mixture was stirred at r.t. for 12 h, filtered and evaporated in vacuum to ~1/3 of its original volume. The resulting yellow precipitate was filtered, washed with methanol (20 mL) and dried at 60 °C to give 495 mg (81% based on **1**) of pure H_2L^1 as a yellow

 This journal is © The Royal Society of Chemistry 2019

Open Access Article. Published on 22 February 2019. Downloaded on 10/24/2025 8:30:16 AM.
This article is licensed under a Creative Commons Attribution 3.0 Unported Licence.

powder. M.p. 184 °C. Elemental analysis for $C_{37}H_{33}NO_5$·1/3MeOH·1/3CH_2Cl_2 (571.67 + 10.68 + 28.32) calcd: C 74.09, H 5.78, N 2.29%; found C 74.24, H 5.43, N 2.17%. *m/z* (ESI−, CH_2Cl_2/MeCN): $C_{37}H_{33}NO_5$ (571.24) $[M - H^+]^-$ calcd: 570.23; found 570.3. ^{1}H-NMR (400 MHz, CH_2Cl_2-d_2, for atom labels see Fig. S13†): δ = 3.38 (d, ^2J = 13.8 Hz, 2H, ArCH_{eq}HAr, $C^{8/14}$), 3.51 (d, ^2J = 13.1 Hz, 2H, ArCH_{eq}HAr, $C^{2/20}$), 3.98 (d, ^2J = 13.8 Hz, 2H, ArCHH_{ax}Ar, $C^{8/14}$), 4.31–4.40 (m, 4H, Ar–CHH_{ax}–Ar, NCH_2, $C^{2/20}$, C^{30}), 4.48 (t, ^3J = 4.9 Hz, 2H, OCH_2, C^{29}), 6.66 (t, ^3J = 7.5 Hz, 2H, *p*-Ar*H*, $C^{5/17}$), 6.67 (t, ^3J = 7.5 Hz, 1H, C^{11}), 6.87–7.02 (m, 7H, *p*-Ar*H*, *m*-Ar*H*, Ar*H* sal, C^{23}, $C^{10/12}$, $C^{6/16}$, C^{34}, C^{36}), 7.07 (dd, ^3J = 7.6 Hz, ^4J = 1.7 Hz, 2H, *m*-Ar*H*, $C^{4/18}$), 7.11 (d, ^3J = 7.6 Hz, 2H, *m*-Ar*H*, $C^{22/24}$), 7.35 (ddd, ^3J = 8.2 Hz, 7.4 Hz, ^4J = 1.7 Hz, 1H, Ar*H* sal, C^{35}), 7.57 (dd, ^3J = 7.6 Hz, ^4J = 1.7 Hz, 1H, Ar*H* sal, C^{33}), 8.81 (s, 1H, C*H*═N, C^{31}). $^{13}C\{^1H\}$ NMR (100 MHz, CH_2Cl_2-d_2, for atom labels see Fig. S13†): δ = 31.8 (Ar*C*H_2Ar, $C^{2/20}$), 32.0 (Ar*C*H_2Ar, $C^{8/14}$), 60.5 (*C*H_2N, C^{30}), 76.5 (O*C*H_2, C^{29}), 117.2 (*C*Ar sal, C^{36}), 119.2 (*C*Ar sal, C^{34}), 119.7 (*C*Ar sal, C^{32}), 121.3 (*p*-*C*Ar c[4]a, $C^{5/17}$), 122.4 (*p*-*C*Ar c[4]a, C^{11}), 126.6 (*p*-*C*Ar c[4]a, C^{23}), 128.6 (*o*-*C*Ar c[4]a, $C^{7/15}$), 128.7 (*o*-*C*Ar c[4]a, $C^{3/19}$), 129.0 (*m*-*C*Ar c[4]a, $C^{4/18}$), 129.2 (*m*-*C*Ar c[4]a, $C^{6/16}$), 129.25 (*m*-*C*Ar c[4]a, $C^{10/12}$), 129.3 (*o*-*C*Ar c[4]a, $C^{9/13}$), 130.0 (*m*-*C*Ar c[4]a, $C^{22/24}$), 132.6 (*C*Ar sal, C^{33}), 133.1 (*C*Ar sal, C^{35}), 134.7 (*o*-*C*Ar c[4]a, $C^{1/21}$), 149.6 (*ipso* *C*Ar–OH c[4]a, C^{27}), 151.5 (*ipso* *C*Ar–OH c[4]a, $C^{26/28}$), 151.7 (*ipso* *C*Ar–O–CH_2 c[4]a, C^{25}), 161.7 (*C*Ar sal, C^{37}), 168.7 (*C*H═N, C^{31}). ATR-IR (ZnSe): ν/cm^{-1} = 3635 (w, νOH), 3500 (w, νOH), 3320 (m, νOH), 3152 (m, νOH), 2952 (w), 2925 (w), 2890 (w), 1635 (s, ν C═N), 1591 (w, νC=C), 1583 (w), 1496 (w), 1464 (s, νC═C), 1448 (s, νC═C), 1429 (m), 1406 (m), 1367 (w), 1337 (w), 1280 (m), 1267 (m), 1246 (m), 1212 (m), 1195 (m), 1150 (m), 1124 (m), 1087 (w), 1058 (w), 1028 (m), 923 (w), 913 (w), 884 (w), 840 (w), 752 (s), 734 (m). UV–vis (MeCN): λ_{max}/nm (ε/M^{-1} cm^{-1}) = 202sh (39 953), 217 (49 380), 254 (13 567), 286 (8882), 311 (6749). This compound was additionally characterized by X-ray crystallography. Crystals suitable for X-ray crystallography were obtained from a solution of H_4L in MeOH.

($HNEt_3$)[Sm_2(HL)(L)] (4). To a solution of H_4L (150 mg, 0.262 mmol) and NEt_3 (0.165 mL, 1.18 mmol) in CH_2Cl_2/MeOH (1/1 : v/v, 30 mL) was added a solution of Sm$(NO_3)_3$·6H_2O (128 mg, 0.289 mmol) at room temperature. The reaction mixture was stirred for 12 h and evaporated to *ca.* 10 mL to give a pale-yellow solid which was isolated by filtration, washed with MeOH (5 mL), and dried at 60 °C. The crude product was further purified by recrystallization from a mixed CH_2Cl_2/EtOH (1 : 1) mixture. Yield: 166 mg (82% based on H_4L). mp > 245 °C (decomposes without melting). *m/z* (ESI−, CH_2Cl_2): $C_{80}H_{75}N_3O_{10}Sm_2$ (1541.385) $[2M - HNEt_3^+]^-$ calcd: 1439.256; found 1439.2; $[M]^-$ calcd 719.124; found 719.1. Found: C 59.57, H 5.12, N 2.70; $C_{80}H_{75}N_3O_{10}Sm_2$·4$H_2O$ (1539.21 + 72.06) requires: C 59.63, H 5.19, N 2.61. AT-IR (ZnSe): ν/cm^{-1} = 3580 (w), 3052 (w), 3025 (w), 2911 (w), 1635 (m, ν C═N), 1593 (w, ν C═C), 1548 (w), 1450 (s, ν C═C), 1427 (m), 1399 (w), 1379 (w), 1316 (w), 1300 (m), 1288 (m), 1266 (w), 1246 (w), 1224 (w), 1186 (m), 1152 (m), 1124 (w), 1087 (m), 1072 (w), 1032 (m), 932 (w), 889 (m), 867 (m), 833 (w), 812 (w), 802 (w), 784 (w), 756 (s), 745 (s), 714 (m), 694 (w). Magnetic moment: $\mu_{eff,dim}$ = 2.40μ_B (per binuclear unit, 300 K), μ_{eff} = 1.70μ_B (per Sm^{3+}). Single crystals of [$HNEt_3$][Sm_2(HL)(L)($MeCN)_2$]·MeCN were grown by diethyl ether vapor diffusion into a acetonitrile solution and analyzed by X-ray diffraction.

($HNEt_3$)[Eu_2(HL)(L)] (5). This compound was prepared from H_4L (150 mg, 0.262 mmol), NEt_3 (0.165 mL, 1.18 mmol), and Eu$(NO_3)_3$·6H_2O (129 mg, 0.289 mmol) in analogy to the samarium compound. Pale-yellow powder. Yield: 140 mg (69% based on H_4L). mp > 245 °C (decomposes without melting). *m/z* (ESI$^-$, CH_2Cl_2/MeCN): $C_{80}H_{75}N_3O_{10}Eu_2$ (1543.388) $[2M - HNEt_3^+]^-$ calcd: 1441.260; found 1441.3; $[M]^-$ calcd 720.126; found 720.1. Found: C 58.54, H 4.98, N 2.62; $C_{80}H_{75}N_3O_{10}Eu_2$·5$H_2O$ (1542.42 + 90.08) requires: C 58.86, H 5.25, N 2.57. AT-IR (ZnSe): ν/cm^{-1} = 3560 (vw), 3051 (w), 3028 (w), 2925 (w), 2914 (w), 1636 (m, ν C═N), 1594 (w, ν C═C), 1548 (w), 1465 (s, ν C═C), 1450 (s, ν C═C), 1427 (m), 1399 (w), 1317 (w), 1300 (m), 1288 (m), 1266 (w), 1246 (w), 1223 (w), 1188 (w), 1154 (w), 1123 (w), 1086 (w), 1071 (w), 1033 (w), 930 (w), 911 (w), 889 (m), 867 (m), 834 (w), 813 (w), 801 (w), 754 (s), 745 (s), 731 (w), 713 (w), 695 (w), 677 (w). Magnetic moment: $\mu_{eff,dim}$ = 4.73μ_B (per binuclear unit, 300 K), μ_{eff} = 3.34μ_B (per Eu^{3+}).

($HNEt_3$)[Gd_2(HL)(L)] (6). H_4L (150 mg, 0.262 mmol), NEt_3 (0.165 mL, 1.18 mmol), and Gd$(NO_3)_3$·6H_2O (130 mg, 0.289 mmol) were reacted in analogy to the procedure detailed above for the europium compound to give 169 mg (83% based on H_4L) of the title compound as pale yellow powder. mp > 240 °C (decomposes without melting). *m/z* (ESI−, CH_2Cl_2): $C_{80}H_{75}N_3O_{10}Gd_2$ (1553.393) $[2M - HNEt_3^+]^-$ calcd: 1451.266; found 1451.3; $[M]^-$ calcd 725.129; found 725.1. Found: C 57.93, H 4.94, N 2.60; $C_{80}H_{75}N_3O_{10}Gd_2$·6$H_2O$ (1552.99 + 108.08) requires: C 57.85, H 5.28, N 2.53. AT-IR (ZnSe): ν/cm^{-1} = 3550 (vw), 3051 (w), 3022 (w), 2905 (w), 1636 (m, ν C═N), 1595 (w, ν C═C) 1582 (m), 1547 (w), 1496 (s, ν C═C), 1454 (s, ν C═C), 1425 (m), 1402 (w), 1325 (m), 1290 (m), 1245 (w), 1222 (w), 1189 (w), 1152 (w), 1085 (w), 1073 (w), 1035 (w), 934 (w), 900 (w), 868 (w), 849 (w), 834 (w), 814 (w), 803 (w), 757 (m), 732 (m), 715 (w). Magnetic moment: $\mu_{eff,dim}$ = 11.37μ_B (per binuclear unit, 300 K), μ_{eff} = 8.04μ_B (per Gd^{3+}). Single crystals of [$HNEt_3$][Gd_2(HL)(L)($MeCN)_2$]·MeCN were grown by diethyl ether vapor diffusion into a acetonitrile solution and analyzed by X-ray diffraction.

($NHEt_3$)[Tb_2(HL)(L)] (7). This compound was prepared from H_4L (150 mg, 0.262 mmol), NEt_3 (0.165 mL, 1.18 mmol), and Tb$(NO_3)_3$·6H_2O (131 mg, 0.289 mmol) in analogy to the samarium compound. Off-white powder. Yield: 157 mg (77% based on H_4L^1). mp > 240 °C (decomposes without melting). *m/z* (ESI−, CH_2Cl_2/MeCN): $C_{80}H_{75}N_3O_{10}Tb_2$ (1555.396) $[2M - HNEt_3^+]^-$ calcd: 1453.268; found 1453.3; $[M]^-$ calcd 726.130; found 726.1. Found: C 56.45, H 4.71, N 2.53; $C_{80}H_{75}N_3O_{10}Tb_2$·$H_2O$·2$CH_2Cl_2$ (1556.34 + 185.92) requires: C 56.47, H 4.68, N 2.41. FT-IR (KBr): ν/cm^{-1} = 3054 (w), 3022 (w), 2998 (w), 2913 (w), 1637 (m, ν C═N), 1596 (w, ν C═C), 1589 (w, ν C═C), 1548 (w), 1466 (s, ν C═C), 1456 (s, ν C═C), 1427 (m), 1440 (w), 1400 (w), 1385 (w), 1326 (w), 1303 (m), 1292 (m),

Open Access Article. Published on 22 February 2019. Downloaded on 10/24/2025 8:30:16 AM.
This article is licensed under a Creative Commons Attribution 3.0 Unported Licence.

1265 (w), 1246 (w), 1224 (w), 1190 (w), 1152 (w), 1125 (w), 1085 (w), 1074 (w), 1049 (w), 1036 (w), 935 (w), 911 (w), 902 (w), 869 (m), 848 (w), 835 (w), 815 (w), 802 (w), 786 (w), 758 (m), 715 (w), 693 (w), 677 (w), 626 (w), 592 (w), 572 (w), 555 (w), 515 (w), 507 (w). Magnetic moment: $\mu_{eff,dim}$ = 13.82μ_B (per binuclear unit, 300 K), μ_{eff} = 9.77μ_B (per Tb^{3+}).

Crystallography

Suitable single crystals of H_2L, $(HNEt_3)[Sm_2(HL)(L)(MeCN)_2]\cdot MeCN$ (**4**·3MeCN), and $(HNEt_3)[Gd_2(HL)(L)(MeCN)_2]\cdot MeCN$ (**6**·3MeCN) were selected and mounted on the tip of a glass fibre using perfluoropolyether oil. The data sets were collected at 180(2) K using a STOE IPDS-2 diffractometer equipped with graphite monochromated Mo-K_α radiation (λ = 0.71073 Å). The data were processed with the programs XAREA.[109] The structure was solved by direct methods[110] and refined by full-matrix least-squares techniques on the basis of all data against F^2 using SHELXL-97.[111] PLATON was used to search for higher symmetry.[112] All non-hydrogen atoms were refined anisotropically. Graphics were produced with Ortep3 for Windows and PovRAY.

Crystal data for $H_4L\cdot 0.5H_2O$. $C_{37}H_{33}NO_{5.5}$, M_r = 579.67 g mol^{-1}, orthorhombic space group $P2_12_12_1$, a = 11.516(2) Å, b = 14.372(3) Å, c = 18.060(4) Å, V = 2989(1) Å^3, Z = 4, ρ_{calcd} = 1.27 g cm^{-3}, T = 181 K, μ(Mo K$_\alpha$) = 0.086 mm^{-1} (λ = 0.71073 Å), 19 399 reflections measured, 5261 unique, 3947 with $I > 2\sigma(I)$. Final R_1 = 0.0317, wR_2 = 0.0757 ($I > 2\sigma(I)$, 393 parameters/0 restraints, min./max. residual electron density = −0.093/0.115 e Å^{-3}. The Flack x parameter (absolute structure parameter) was calculated to be −0.36(16) for the present structure and 1.36 for the inverted structure. The solvate molecule is disordered over two positions with site occupancy factors of 0.25 each (fixed). Hydrogen atoms were not calculated for this solvate molecule.

Crystal data for $(HNEt_3)[Sm_2(HL)(L)(MeCN)_2]\cdot MeCN$. $C_{87}H_{85.5}N_{6.5}O_{10}Sm_2$, M_r = 1662.37 g mol^{-1}, orthorhombic space group $Pbca$, a = 22.6899(5) Å, b = 25.2258(5) Å, c = 26.5373(5) Å, V = 15 189.2(5) Å^3, Z = 8, ρ_{calcd} = 1.466 g cm^{-3}, T = 180(2) K, μ(Mo K$_\alpha$) = 1.595 mm^{-1} (λ = 0.71073 Å), 48 009 reflections measured, 14 906 unique, 11 481 with $I > 2\sigma(I)$. Final R_1 = 0.0416, wR_2 = 0.1137 ($I > 2\sigma(I)$, 945 parameters/0 restraints, min./max. residual electron density = −0.611/1.995 e Å^{-3}. The N–H hydrogen atom of the $HNEt_3^+$ cation and the OH hydrogen atom of the $[Sm_2(HL)(L)(MeCN)_2]^-$ anion were located unambiguously from final Fourier maps but were refined using a riding model.

Crystal data for $(HNEt_3)[Gd_2(HL)(L)(MeCN)_2]\cdot MeCN$. $C_{86}H_{84}Gd_2N_6O_{10}$ M_r = 1676.15 g mol^{-1}, orthorhombic space group $Pbca$, a = 22.7767(8) Å, b = 25.1415(11) Å, c = 26.5012(10) Å, V = 15 175.7(10) Å^3, Z = 8, ρ_{calcd} = 1.466 g cm^{-3}, T = 180(2) K, μ(Mo K$_\alpha$) = 1.797 mm^{-1} (λ = 0.71073 Å), 51 122 reflections measured, 16 712 unique, 10 439 with $I > 2\sigma(I)$. Final R_1 = 0.0485, wR_2 = 0.1160 ($I > 2\sigma(I)$, 942 parameters/6 restraints, min./max. residual electron density = −0.838/1.115 e Å^{-3}.

CCDC 1880057 (H_4L), 1880058 (**4**) and 1880059 (**6**)† contain the supplementary crystallographic data for this paper.

Spectrophotometric titrations/determination of stability constants

A series of UV-vis spectroscopic studies were performed in order to determine the composition and stability constants of the lanthanide complexes. The stoichiometry of the lanthanide complexes was determined by the mole ratio method. All titrations were performed at 298 K in Hellma 110-QS quartz cells of 1 cm optical path length containing solutions at constant ionic strength ($N(nBu)_4PF_6$ 0.01 M) and constant ligand concentrations (5 × 10^{-5} M) in MeCN. For each experiment, 21 solutions were prepared by combining stock solutions of the ligand and the corresponding $Ln(NO_3)_3\cdot 6H_2O$ salts with an Eppendorf micropipette (volume range of 10–100 μL and 100–1000 μL; 0.71–0.10% error) and allowed to stir for 12 h. UV–vis absorption spectra were collected in the 190–650 nm range at uniform data point intervals of 1 nm with a double-beam V-670 (Jasco) spectrophotometer. The multiwavelength data sets were analyzed by a nonlinear least-squares procedure implemented in the Hyperquad2008 v1.1.33 software.

Synthesis of the polycarbonate films

Polycarbonate Z200 (0.30 g) was dissolved in CH_2Cl_2 (1.5 mL) and stirred for 10 min. A solution of the lanthanide complex (V = 1 mL, 8 × 10^{-3} M) in CH_2Cl_2 was added to the PC solution. The resulting mixture was spread on a Petri dish (d = 5 cm) and the solvent was allowed to evaporate in open air over night.

Luminescence lifetime measurements

The luminescence lifetime of the Tb complex **7** was measured applying a Fluoromax4 (HoribaScientific) equipped with a Fluorohub (Horiba Scientific) and the DataStation (Version 2.7) software package for TCSPC applications. The sample, imbedded in a thin polycarbonate matrix, was installed at an 35° angle towards the incident excitation light beam. Excitation and emission wavelengths of 310 and 545 nm were chosen. The time resolution was 1.33 μs per channel. In order to determine the instrument response function we used the identical setup with a highly reflective spectralon sample. The photon count rate was well below 1 percent of the excitation count rate ruling out pile up effects.

Conflicts of interest

There are no conflicts of interest to declare.

Acknowledgements

We are thankful to Prof. Dr H. Krautscheid for providing facilities for X-ray crystallographic measurements. Financial support from the German Federal Ministry of Education and Research (BMBF – project 02NUK046C) and the Deutsche Forschungsgemeinschaft (DFG – Priority Program SPP2102,

Open Access Article. Published on 22 February 2019. Downloaded on 10/24/2025 8:30:16 AM.
This article is licensed under a Creative Commons Attribution 3.0 Unported Licence.

"Light Controlled Reactivity of Metal Complexes") is gratefully acknowledged.

References

1 D. Gutsche, *Calixarenes: An Introduction*, RSC Publishing, Cambridge, 2nd edn, 2008.
2 V. Böhmer, *Angew. Chem.*, 1995, **107**, 785–818, (*Angew. Chem., Int. Ed. Engl.*, 1995, **34**, 713–745).
3 R. Kumar, Y. Jung and J. S. Kim, in *Calixarenes and Beyond*, ed. P. Neri, J. L. Sessler and M.-X. Wang, Springer, 2016.
4 C. Wieser, C. B. Dieleman and D. Matt, *Coord. Chem. Rev.*, 1997, **165**, 93–161.
5 P. D. Beer and E. J. Hayes, *Coord. Chem. Rev.*, 2003, **240**, 167–189.
6 C. Redshaw, *Coord. Chem. Rev.*, 2003, **244**, 45–70.
7 C. J. Elsevier, J. Reedijk, P. H. Walton and M. D. Ward, *Dalton Trans.*, 2003, 1869–1880.
8 W. Sliwa, *J. Inclusion Phenom. Macrocyclic Chem.*, 2005, **52**, 13–37.
9 A. Casnati, N. Della Ca', M. Fontanella, F. Sansone, F. Ugozzoli, R. Ungaro, K. Liger and J.-F. Dozol, *Eur. J. Org. Chem.*, 2005, 2338–2348.
10 J. Vicens and J. Harrowfield, *Calixarenes in the Nanoworld*, Springer, Netherlands, 2007.
11 B. S. Creaven, D. F. Donlon and J. McGinley, *Coord. Chem. Rev.*, 2009, **253**, 893–962.
12 L. Baldini, F. Sansone, A. Casnati and R. Ungaro, Calixarenes in Molecular Recognition, in *Supramolecular Chemistry: From Molecules to Nanomaterials*, ed. P. A. Gale and J. W. Steed, John Wiley & Sons, 2012, vol. 3.
13 R. Gramage-Doria, D. Armspach and D. Matt, *Coord. Chem. Rev.*, 2013, **257**, 776–816.
14 D. Semeril and D. Matt, *Coord. Chem. Rev.*, 2014, **279**, 58–95.
15 D. M. Homden and C. Redshaw, *Chem. Rev.*, 2008, **108**, 5086–5130.
16 A. B. Chetry, T. Matsufuji, B. B. Adhikari, S. Morisada, H. Kawakita, K. Ohto, T. Oshima and Jumina, *J. Inclusion Phenom. Macrocyclic Chem.*, 2015, **81**, 301–310.
17 J.-N. Rebilly, B. Colasson, O. Bistri, D. Over and O. Reinaud, *Chem. Soc. Rev.*, 2015, **44**, 467–489.
18 M. A. McKervey, F. Arnaud-Neu and M.-J. Schwing-Weill, in *Comprehensive Supramolecular Chemistry*, ed. G. Gokel, Pergamon, Oxford, 1996.
19 J. M. Harrowfield, M. I. Ogden and A. H. White, *J. Chem. Soc., Dalton Trans.*, 1991, 2625–2632.
20 P. D. Beer, M. G. B. Drew, M. Kan, P. B. Leeson, M. I. Ogden and G. Williams, *Inorg. Chem.*, 1996, **35**, 2202–2211.
21 A. Casnati, L. Baldini, F. Sansone, R. Ungaro, N. Armaroli, D. Pompei and F. Barigelletti, *Supramol. Chem.*, 2002, **14**, 281–289.
22 G. Guillemot, B. Castellano, T. Prangé, E. Solari and C. Floriani, *Inorg. Chem.*, 2007, **46**, 5152–5154.
23 G. B. Deacon, M. G. Gardiner, P. C. Junk, J. P. Townley and J. Wang, *Organometallics*, 2012, **31**, 3857–3864.
24 B. M. Furfy, J. M. Harrowfield, D. L. Kepert, B. W. Skelton, A. H. White and F. R. Wilner, *Inorg. Chem.*, 1987, **26**, 4231–4236.
25 S. Barboso, A. G. Carrera, S. E. Matthews, F. Arnaud-Neu, V. Böhmer, J.-F. Dozol, H. Rouquette and M.-J. Schwing-Weill, *J. Chem. Soc., Perkin Trans. 2*, 1999, 719–724.
26 R. Ludwig, *Fresenius' J. Anal. Chem.*, 2000, **376**, 103–128.
27 J. F. Dozol and R. Ludwig, *Ion Exch. Solvent Extr.*, 2010, **19**, 195–318.
28 I. Vatsouro, A. Serebryannikova, L. Wang, V. Hubscher-Bruder, E. Shokova, M. Bolte, F. Arnaud-Neu, V. Böhmer and V. Kovalev, *Tetrahedron*, 2011, **67**, 8092–8101.
29 F. de María Ramírez, S. Varbanov, J.-C. G. Bünzli and R. Scopelliti, *Inorg. Chim. Acta*, 2011, **378**, 163–168.
30 D. R. Raut, P. K. Mohapatra, S. A. Ansari, S. V. Godbole, M. Iqbal, D. Manna, T. K. Ghanty, J. Huskens and W. Verboom, *RSC Adv.*, 2013, **3**, 9296–9303.
31 M. Atanassova and V. Kurteva, *RSC Adv.*, 2016, **6**, 11303–11324.
32 S. A. Ansari, P. K. Mohapatra, S. M. Ali, A. Sengupta, A. Bhattacharyya and W. Verboom, *Dalton Trans.*, 2016, **45**, 5425–5429.
33 S. A. Ansari, P. K. Mohapatra, W. Verboom, Z. Zhang, P. D. Dau, J. K. Gibson and L. Rao, *Dalton Trans.*, 2015, **44**, 6416–6422.
34 A. Leydier, D. Lecerclé, S. Pellet-Rostaing, A. Favre-Réguillon, F. Taran and M. Lemaire, *Tetrahedron*, 2008, **64**, 11319–11324.
35 D. N. Woodruff, R. E. P. Winpenny and R. A. Layfield, *Chem. Rev.*, 2013, **113**, 5110–5148.
36 J. S. Kim and D. T. Quang, *Chem. Rev.*, 2007, **107**, 3780–3799.
37 D. D'Alessio, S. Muzzioli, B. W. Skelton, S. Stagni, M. Massi and M. I. Ogden, *Dalton Trans.*, 2012, **41**, 4736–4739.
38 C. R. Driscoll, B. W. Skelton, M. Massi and M. I. Ogden, *Supramol. Chem.*, 2016, **28**, 567–574.
39 S. J. Butler and D. Parker, *Chem. Soc. Rev.*, 2013, **42**, 1652–1666.
40 M. L. Aulsebrook, B. Graham, M. R. Grace and K. L. Tuck, *Coord. Chem. Rev.*, 2018, **375**, 191–220.
41 N. Sabbatini, M. Guardigli, A. Mecati, V. Balzani, R. Ungaro, E. Ghidini, A. Casnati and A. Pochini, *J. Chem. Soc., Chem. Commun.*, 1990, 878–879.
42 N. Sato, I. Yoshida and S. Shinkai, *Chem. Lett.*, 1993, 621–624.
43 F. J. Steemers, W. Verboom, D. N. Reinhoudt, E. B. van der Tol and J. W. Verhoeven, *J. Am. Chem. Soc.*, 1995, **117**, 9408–9414.
44 B. W. Ennis, S. Muzzioli, B. L. Reid, D. D'Alessio, S. Stagni, D. H. Brown, M. I. Ogden and M. Massi, *Dalton Trans.*, 2013, **42**, 6894–6901.

Open Access Article. Published on 22 February 2019. Downloaded on 10/24/2025 8:30:16 AM.
This article is licensed under a Creative Commons Attribution 3.0 Unported Licence.

45 M. Massi and M. I. Ogden, *Materials*, 2017, **10**, 1369–1381.
46 C. Lincheneau, E. Quinlan, J. A. Kitchen, T. McCabe, S. E. Matthews and T. Gunnlaugsson, *Supramol. Chem.*, 2013, **25**, 869–880.
47 M. J. McIldowie, B. W. Skelton, M. Mocerino and M. I. Ogden, *J. Inclusion Phenom. Macrocyclic Chem.*, 2015, **82**, 43–46.
48 P. D. Beer, M. G. B. Drew and M. I. Ogden, *J. Chem. Soc., Dalton Trans.*, 1997, 1489–1492.
49 C. R. Driscoll, B. L. Reid, M. J. McIldowie, S. Muzzioli, G. L. Nealon, B. W. Skelton, S. Stagni, D. H. Brown, M. Massi and M. I. Ogden, *Chem. Commun.*, 2011, **47**, 3876–3878.
50 F. Glasneck, K. Kobalz and B. Kersting, *Eur. J. Inorg. Chem.*, 2016, 3111–3122.
51 R. K. Pathak, A. G. Dikundwar, T. N. Guru Row and C. P. Rao, *Chem. Commun.*, 2010, **46**, 4345–4347.
52 R. K. Pathak, V. K. Hinge, M. Mondal and C. P. Rao, *J. Org. Chem.*, 2011, **76**, 10039–10049.
53 R. Joseph, J. P. Chinta and C. P. Rao, *Inorg. Chem.*, 2011, **50**, 7050–7058.
54 V. V. S. Mummidivarapu, V. K. Hinge and C. P. Rao, *Dalton Trans.*, 2015, **44**, 1130–1141.
55 R. K. Pathak, V. K. Hinge, A. Rai, D. Panda and C. P. Rao, *Inorg. Chem.*, 2012, **51**, 4994–5005.
56 S. Ullmann, R. Schnorr, M. Handke, C. Laube, B. Abel, J. Matysik, M. Findeisen, R. Rüger, T. Heine and B. Kersting, *Chem. – Eur. J.*, 2017, **23**, 3824–3827.
57 S. Ullmann, R. Schnorr, C. Laube, B. Abel and B. Kersting, *Dalton Trans.*, 2018, **47**, 5801–5811.
58 W.-C. Zhang and Z.-T. Huang, *Synthesis*, 1997, 1073–1076.
59 K. Nakamoto, *Infrared and Raman Spectra of Inorganic and Coordination Compounds*, Wiley, Hoboken, New Jersey, 6th edn, 2009, part B.
60 J. U. Ahmad, M. Nieger, M. R. Sundberg, M. Leskelä and T. Repo, *J. Mol. Struct.*, 2011, **995**, 9–15.
61 C. Jaime, J. de Mendoza, P. Prados, P. M. Nieto and C. Sanchez, *J. Org. Chem.*, 1991, **56**, 3372–3376.
62 Y. Liu, B.-T. Zhao, H.-Y. Zhang, T. Wada and Y. Inoue, *J. Chem. Soc., Perkin Trans. 2*, 2001, 1219–1223.
63 S. R. Menon and J. A. R. Schmidt, *Tetrahedron*, 2016, **72**, 767–774.
64 L. J. Charbonnière, C. Balsiger, K. J. Schenk and J.-C. G. Bünzli, *J. Chem. Soc., Dalton Trans.*, 1998, 505–510.
65 M. La Deda, M. Ghedini, I. Aiello and A. Grisolia, *Chem. Lett.*, 2004, **33**, 1060–1061.
66 R. D. Archer, H. Chen and L. C. Thompson, *Inorg. Chem.*, 1998, **37**, 2089–2095.
67 A. Filarowski, *J. Phys. Org. Chem.*, 2005, **18**, 686–698.
68 I. Kaljurand, A. Kütt, L. Sooväli, T. Rodima, V. Mäemets, I. Leito and I. A. Koppel, *J. Org. Chem.*, 2005, **70**, 1019–1028.
69 K. Nakamoto, *Infrared and Raman Spectra of Inorganic and Coordination Compounds*, John Wiley & Sons, Inc., Hoboken, New Jersey, 6th edn, 2009, part B.
70 W. Xu, R. J. Puddephatt, L. Manojlovic-Muir, K. W. Muir and C. S. Frampton, *J. Inclusion Phenom. Mol. Recognit. Chem.*, 1994, **19**, 277–290.
71 P. Thuéry, Z. Asfari, M. Nierlich and J. Vicens, *Acta Crystallogr., Sect. C: Cryst. Struct. Commun.*, 2002, **58**, o223–o225.
72 J. M. Harrowfield, M. I. Ogden and A. H. White, *Aust. J. Chem.*, 1991, **44**, 1237–1247.
73 S. Fleming, C. D. Gutsche, J. M. Harrowfield, M. I. Ogden, B. W. Skelton, D. F. Stewart and A. H. White, *Dalton Trans.*, 2003, 3319–3327.
74 B. M. Furthy, J. M. Harrowfield, M. I. Ogden, B. W. Skelton, A. H. White and F. R. Wilner, *J. Chem. Soc., Dalton Trans.*, 1989, 2217–2221.
75 I. D. Brown, *Acta Crystallogr., Sect. A: Cryst. Phys., Diffr., Theor. Gen. Crystallogr.*, 1976, **32**, 24–31.
76 G. A. Jeffrey, *An Introduction to Hydrogen Bonding*, Oxford University Press, Oxford, UK, 1997.
77 T. Steiner, *Angew. Chem.*, 2002, **114**, 50–80, (*Angew. Chem., Int. Ed.*, 2002, **41**, 48–76).
78 G. L. Nealon, M. Mocerino, M. I. Ogden and B. W. Skelton, *J. Inclusion Phenom. Macrocyclic Chem.*, 2009, **65**, 25–30.
79 R. D. Shannon, *Acta Crystallogr., Sect. A: Cryst. Phys., Diffr., Theor. Gen. Crystallogr.*, 1976, **32**, 751–767.
80 M. Andruh, E. Bakalbassis, O. Kahn, J.-C. Trombe and P. Porcher, *Inorg. Chem.*, 1993, **32**, 1616–1622.
81 A. F. Orchard, *Magnetochemistry*, Oxford University Press, Oxford, 2007.
82 J.-P. Costes, F. Dahan, A. Dupuis, S. Lagrave and J.-P. Laurent, *Inorg. Chem.*, 1998, **37**, 153–155.
83 J. Long, F. Habib, P.-H. Lin, I. Korobkov, G. Enright, L. Ungur, W. Wernsdorfer, L. F. Chibotaru and M. Murugesu, *J. Am. Chem. Soc.*, 2011, **133**, 5319–5328.
84 P.-H. Lin, M. Leclère, J. Long, T. J. Burchell, I. Korobkov, R. Clérac and M. Murugesu, *Dalton Trans.*, 2010, **39**, 5698–5704.
85 P. Comba, M. Großhauser, R. Klingeler, C. Koo, Y. Lan, D. Müller, J. Park, A. Powell, M. J. Riley and H. Wadepohl, *Inorg. Chem.*, 2015, **54**, 11247–11258.
86 L. E. Roy and T. Hughbanks, *J. Am. Chem. Soc.*, 2006, **128**, 568–575.
87 S. Liu, L. Gelmini, S. J. Rettig, R. C. Thompson and C. Orvig, *J. Am. Chem. Soc.*, 1992, **114**, 6081–6087.
88 J. H. Van Vleck and A. Frank, *Phys. Rev.*, 1929, **34**, 1494–1499.
89 A. Jäschke, M. Kischel, A. Mansel and B. Kersting, *Eur. J. Inorg. Chem.*, 2017, 894–901.
90 J.-X. Xu, Y. Ma, D. Liao, G.-F. Xu, J. Tang, C. Wang, N. Zhou, S.-P. Yan, P. Cheng and L.-C. Li, *Inorg. Chem.*, 2009, **48**, 8890–8896.
91 M. Reng, Z.-L. Xu, S.-S. Bao, T.-T. Wang, Z.-H. Zheng, R. A. Ferreira, L.-M. Zheng and L. D. Carlos, *Dalton Trans.*, 2016, 2974–2982.
92 J. H. Yoe and A. E. Harvey, *J. Am. Chem. Soc.*, 1948, **70**, 648–654.
93 P. Di Bernardo, A. Melchior, M. Tolazzi and P. L. Zanonato, *Coord. Chem. Rev.*, 2012, **256**, 328–351.

 This journal is © The Royal Society of Chemistry 2019

Open Access Article. Published on 22 February 2019. Downloaded on 10/24/2025 8:30:16 AM.
This article is licensed under a Creative Commons Attribution 3.0 Unported Licence.

94 A. F. Danil de Namor and O. Jafou, *J. Phys. Chem. B*, 2001, **105**, 8018–8027.
95 P. M. Marcos, J. R. Ascenso, M. A. P. Segurado, P. J. Cragg, S. Michel, V. Hubscher-Bruder and F. Arnaud-Neu, *Supramol. Chem.*, 2011, **23**, 93–101.
96 P. M. Marcos, J. D. Fonseca, C. S. Proença, J. R. Ascenso, R. J. Bernardino, J. Kulesza and M. Bochenska, *Supramol. Chem.*, 2016, **28**, 367–376.
97 A. F. Danil de Namor, K. Baron, S. Chahine and O. Jafou, *J. Phys. Chem. A*, 2004, **108**, 1082–1089.
98 N. E. Borisova, A. A. Kostin, E. A. Eroshkina, M. D. Reshetova, K. A. Lyssenko, E. N. Spodine and L. N. Puntus, *Eur. J. Inorg. Chem.*, 2014, **2014**, 2219–2229.
99 The Sm complex **4** is not emissive at 77 K neither in solution nor in polycarbonate.
100 K. Binnemans, *Coord. Chem. Rev.*, 2015, **295**, 1–45.
101 A. E. V. Gorden, J. D. Xu, K. N. Raymond and P. Durbin, *Chem. Rev.*, 2003, **103**, 4207–4282.
102 G. Vicentini, L. B. Zinner, J. Zukerman-Schpector and K. Zinner, *Coord. Chem. Rev.*, 2000, **196**, 353–382.
103 M. Hilder, P. C. Junk, U. H. Kynast and M. M. Lezhnina, *J. Photochem. Photobiol., A*, 2009, **202**, 10–20.
104 J.-C. G. Bünzli and S. Eliseeva, Basics of Lanthanide Photophysics, in *Lanthanide Luminescence*, ed. P. Hänninen and H. Härmä, Springer Berlin Heidelberg, Berlin, 2011, vol. 7, pp. 1–45.
105 D. Parker, *Coord. Chem. Rev.*, 2000, **205**, 109–130.
106 N. Felorzabihi, J. C. Haley, G. R. Bardajee and M. A. Winnik, *J. Polym. Sci., Part B: Polym. Phys.*, 2007, **45**, 2333–2343.
107 A. T. Bui, A. Grichine, A. Duperray, P. Lidon, F. Riobé, C. Andraud and O. Maury, *J. Am. Chem. Soc.*, 2017, **139**, 7693–7696.
108 M. Strobel, K. Kita-Tokarczyk, A. Taubert, C. Vebert, P. A. Heiney, M. Chami and W. Meier, *Adv. Funct. Mater.*, 2006, **16**, 252–259.
109 Stoe & Cie, *X-AREA and X-RED 32; V1.35*, Stoe & Cie, Darmstadt, Germany, 2006.
110 G. M. Sheldrick, *Acta Crystallogr., Sect. A: Found. Crystallogr.*, 1990, **46**, 467–473.
111 G. M. Sheldrick, *SHELXL-97, Computer program for crystal structure refinement*, University of Göttingen, Göttingen, Germany, 1997.
112 A. L. Spek, *PLATON - A Multipurpose Crystallographic Tool*, Utrecht University, Utrecht, The Netherlands, 2000.